



Accepted Article

Title: Nonlinear unmixing of hyperspectral datasets for the study of painted works of art

Authors: Neda Rohani, Emeline Pouyet, Oliver Cossairt, Aggelos Katsaggelos, and Marc Walton

This manuscript has been accepted after peer review and appears as an Accepted Article online prior to editing, proofing, and formal publication of the final Version of Record (VoR). This work is currently citable by using the Digital Object Identifier (DOI) given below. The VoR will be published online in Early View as soon as possible and may be different to this Accepted Article as a result of editing. Readers should obtain the VoR from the journal website shown below when it is published to ensure accuracy of information. The authors are responsible for the content of this Accepted Article.

To be cited as: *Angew. Chem. Int. Ed.* 10.1002/anie.201805135 *Angew. Chem.* 10.1002/ange.201805135

Link to VoR: http://dx.doi.org/10.1002/anie.201805135 http://dx.doi.org/10.1002/ange.201805135

COMMUNICATION WILEY-VCH

Nonlinear unmixing of hyperspectral datasets for the study of painted works of art

Neda Rohani [a], Emeline Pouvet[b], Marc Walton* [b], Oliver Cossairt[a], Aggelos K. Katsaggelos[a]

Abstract: Nonlinear unmixing of hyperspectral reflectance data is one of the key problems in quantitative imaging of painted works of art. Our approach is to interrogate a hyperspectral image cube by, first, decomposing it into a set of reflectance curves representing pure basis pigments and, second, to estimate the scattering and absorption coefficients of each pigment in a given pixel to produce estimates of the component fractions. This two-step algorithm uses i) a deep neural network to qualitatively identify the constituent pigments in any unknown spectrum and, based on the pigment(s) present, ii) Kubelka-Munk theory to estimate the pigment concentration on a perpixel basis. Using hyperspectral data acquired on a set of mockup paintings and a well-characterized illuminated folio from the 15th century, we demonstrate the performance of the proposed algorithm for pigment recognition and quantitative estimation of concentration.

Pigment identification allows for an understanding of how artists/workshops used their materials, how painted surfaces may chemically change over time, and, lastly, how anachronistic uses of materials can be associated with either fakes/forgeries or past restorations. A primary tool for these tasks is hyperspectral imaging (HSI), a fast non-invasive and *in-situ* method that has become commonplace in cultural heritage to document the distribution of pigments across painted surfaces, especially when employed together with complementary analytical techniques. [1-11]

Pigment mixture identification from HSI datasets is an ongoing challenge. It usually combines non-automated data interpretation (namely, a simple visual comparison to literature reflectance data) and classification algorithms. Mapping pigments with HSI datasets is achieved by linear spectral unmixing methods, e.g., maximum-likelihood estimation, spectral angle mapping, subspace projection methods, or constrained least squares. These approaches consider the spectrum as a linear combination of two or more endmembers, defined as a spectrum representing a pure pigment. While linear unmixing is computationally fast and easy to implement, pigment mixtures have a non-linear reflectance response. [12] For this reason, most of the conventional approaches for spectral unmixing do not provide accurate estimates of pigment concentration on painted surfaces.

Significant limitations imposed by linear unmixing may be overcome by approximating the reflectance from mixed pigments through a simplified Kubelka-Munk (KM) model for opaque and infinitely thick samples. [12-14] Using single or two-constant KM models, the non-linearity of pigment mixtures has previously been modeled. [3,15-20] In these studies, the pure pigments best explaining spectral features are combined following KM theory to create libraries of computed spectra. This database is then matched to the experimental data using linear regression. [21] To date, the use of KM modeling on a per pixel basis has been performed on a limited number of mock-up datasets to demonstrate proof of concept but is generally considered too computationally intensive for practical use.

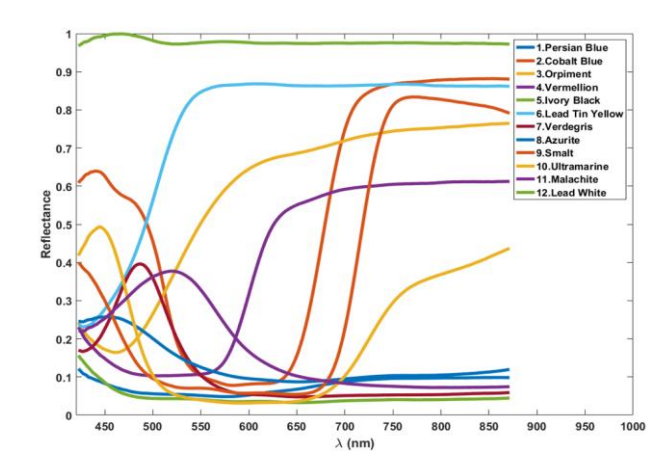


Figure 1. Reflectance spectra of 12 single pigment paint layers from the dataset.

Previous attempts to overcome computational bottlenecks using single-constant KM modeling have relied on chromatic segmentation and clustering as preliminary measures to reduce the total number of spectra being fitted.^[20,22]

In this work, a pixel-wise unmixing problem is solved to produce semi-quantitative maps of pigment distributions. We are inspired by recent work that developed a multilayer perceptron neural network for classifying pigments, [23] as well as studies from the field of remote sensing in which convolutional neural networks, stacked auto-encoders, deep belief networks, and restricted Boltzmann machines have been used for feature extraction, [24-25] classification [26-29] and unmixing. [30] In this study, pigments present in a given spectrum are identified using a deep neural network designed to perform supervised classification. Having found the pigments in each pixel, the concentration values of the individual components are estimated, on a pixel-by-pixel basis, using a KM model and non-linear optimization (more specifically, a gradient descent algorithm).

Mock-ups were prepared to build and test the computational efficiency, accuracy, and precision of the developed model. The choice of pigments was based on analysis of an illuminated manuscript currently housed at the Isabella Stewart Gardner Museum (Ms. 6.T.6) which served as a test case for the algorithm described. The mock-up is composed of 12 pure pigments (the average spectra of the pure pigments in the reflectance domain are presented in Fig. 1) and, 16 of two and three pigment mixtures. The pigment weight ratio percentages were (i) 50/50 for the two pigments mixture, and (ii) 33/33/33 for the three pigments mixture (more details about sample preparation are given in [31] and sec. A, table 2 in the supplementary material).

From the known and controlled composition of the mock-up paint layers, the following methodology was developed as shown in Fig. 2 and enumerated below:

COMMUNICATION WILEY-VCH

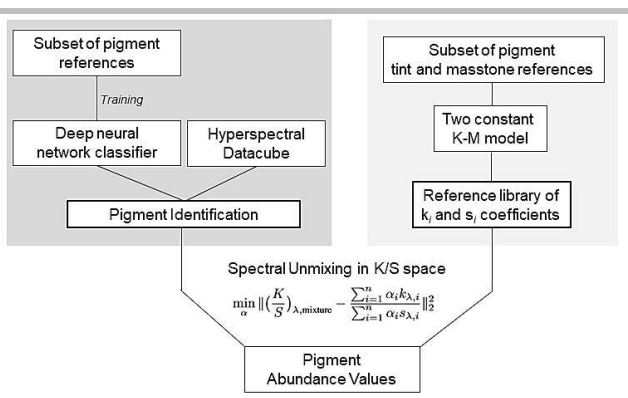


Figure 2. Algorithm flowchart.

Step 1: Using the reflectance spectra from single colored pigments and 50/50 mixture of lead white and colored pigments, a two-constant KM model is applied to calculate the absorption $k_{\lambda,i}$, and scattering, $s_{\lambda,i}$ coefficients of each pigment. For a detailed description of these calculations please refer to Berns [18] and to supplementary material (sec. B, eqs. 3-4).

Step 2: The pigments present in a given pixel are identified using a deep feed-forward neural network. Here, the problem is posed as either a multi-class [32] classification task. [33] Additional details regarding classification schemes are given in the supporting material (sec. C and table 2). Multi-label classification task is more suitable for real datasets where not all possible mixtures are known (results shown in sec. D and table 3 in the supplementary material).

Step 3: KM is used to model the observed reflectance spectrum given inputs from steps 1 and 2 (Eq. 2 in sec. B). A gradient descent KM solver (Eq. 2 in sec. B) provides an estimation of pigment concentrations. The KM solver is used in combination with a constrained nonlinear multivariable optimization function that minimizes the reconstruction error between the experimental spectrum and reconstructed one (Eq. 10 in sec. E). The minimization is subject to two constraints on the concentration values, that is, abundances need to sum to one and abundances are non-negative (more details about gradient descent method are given in [34-35] and in sec. E).

The results from this workflow may be observed in table 1 where average weight fractions are compared to their true abundances for mock-up mixtures of i) Verdigris with Lead White, ii) Lead Tin Yellow with Verdigris and Malachite, iii) Verdigris with Malachite and iv) Azurite with Ultramarine. For combinations of two and three colors, the estimated abundances are respectively equal to 0.50 ± 0.15 and 0.33 ± 0.17 . These measured data closely approximate their ground truth abundances thus indicating the efficacy of the three-step nonlinear unmixing approach for the quantitative analysis of historical paint mixtures.

To test our approach on more complex works of art, suffrages from the Gardner Museum's 15th century book of hours were studied using a combination of both HSI and macro X-Ray Fluorescence (XRF) spectroscopy. We chose to focus on a single page of the full book (page 34v, Fig. 3a).^[31] The complete experimental acquisition setup is given in supplementary material (sec. A). Pigment distribution maps were obtained following the three-step strategy described above and presented in Fig. 3b.

Table 1. Ground truth compared to proposed approach estimated abundance fractions by weight

	Ground truth	Proposed Method		
Mixture	abundance fraction by weight	Average	Standard Deviation	
Verdigris	0.50	0.51	0.01	
Lead White	0.50	0.49	0.01	
Lead Tin Yellow	0.33	0.34	0.17	
Verdigris	0.33	0.32	0.16	
Malachite	0.33	0.34	0.17	
Verdigris	0.50	0.49	0.15	
Malachite	0.50	0.51	0.15	
Azurite	0.50	0.51	0.15	
Ultramarine	0.50	0.49	0.15	

The red mantle of the central figure and red flowers in the decoration area (Fig. 3b) contain high amounts of the pigment vermilion (HgS). The spectra of these areas have sigmoidal shapes with a steep rise and an inflection point centered at 590-605 nm characteristic of the pigment. [36-37] This concentration distribution information is confirmed by XRF results that show the presence of mercury and sulfur in a similar area (Fig. 3c). From the HSI information, vermilion is present as a pure single pigment in the flower (point 1, (Fig. 4b and c), but is mixed with a small amount of lead white (0-30%) in the mantle area.

The presence of the pigment hematite (Fe_2O_3) is determined in two interior framing lines of the page (Fig. 3b). The spectra from these regions that match hematite reflectance references show an inflection peak at 580 nm, a minor reflectance peak at ~600 nm, and a more pronounced peak one at ~750nm (Fig. 4b and c).[36-37] Iron is also confirmed by XRF analyses however the spatial resolution offered by this method alone did not allow to propose accurate location of the framing lines compared to the HSI data (Fig. 3c).

The pigment ultramarine (Na $_8$ [Al $_6$ Si $_6$ O $_{24}$]S $_n$, the mineral lazurite) is identified in the blue dress, with a reflectance spectrum characterized by a maximum of absorption at 600 nm and a transition to high reflectance around 700 nm. In the blue flowers, the presence of azurite (2CuCO $_3$.Cu(OH) $_2$) mixed with ultramarine is observed, this is confirmed by a decrease in reflectance between 700 and 900 nm (Fig. 4b). [37] XRF spectra confirm a significant amount of Cu, consistent with the presence of azurite, together with Al, Si and K, all of which confirm the presence of ultramarine (Fig. 3c).

Together with lead white, different shades and hues of blue can be achieved as observed in the RGB image of the illumination. Using our KM approach, the different ratios of ultramarine, azurite and lead white used to paint these decorations were estimated. In the darker area of the paint, ultramarine solely is identified. This layer is applied on top of the light blue paint. However, in a single stroke of the light blue paint, azurite is identified together with ultramarine and lead white (as an example, point 3 presents 36% azurite, 23% ultramarine, and 41% lead white by weight- Fig. 4b and c). As has been found previously [38], ultramarine was intentionally layered over azurite to create deeper blue hues. The identification of azurite and ultramarine intimately mixed in the light blue tones of this manuscript is unusual but shows the power of our quantitative technique in teasing apart such subtle mixtures.

 [[]a] N. Rohani, Dr. O. Cossairt, Dr. A. K. Katsaggelos
 Department of Electrical Engineering and Computer Science,
 Northwestern University, Evanston, IL, USA

 [[]b] Dr. E. Pouyet, Dr. M. Walton Center for Scientific Studies in the Art, Northwestern University, Evanston, IL, USA

^{*}Corresponding author email: E-mail: marc.walton@northwstern.edu

COMMUNICATION WILEY-VCH

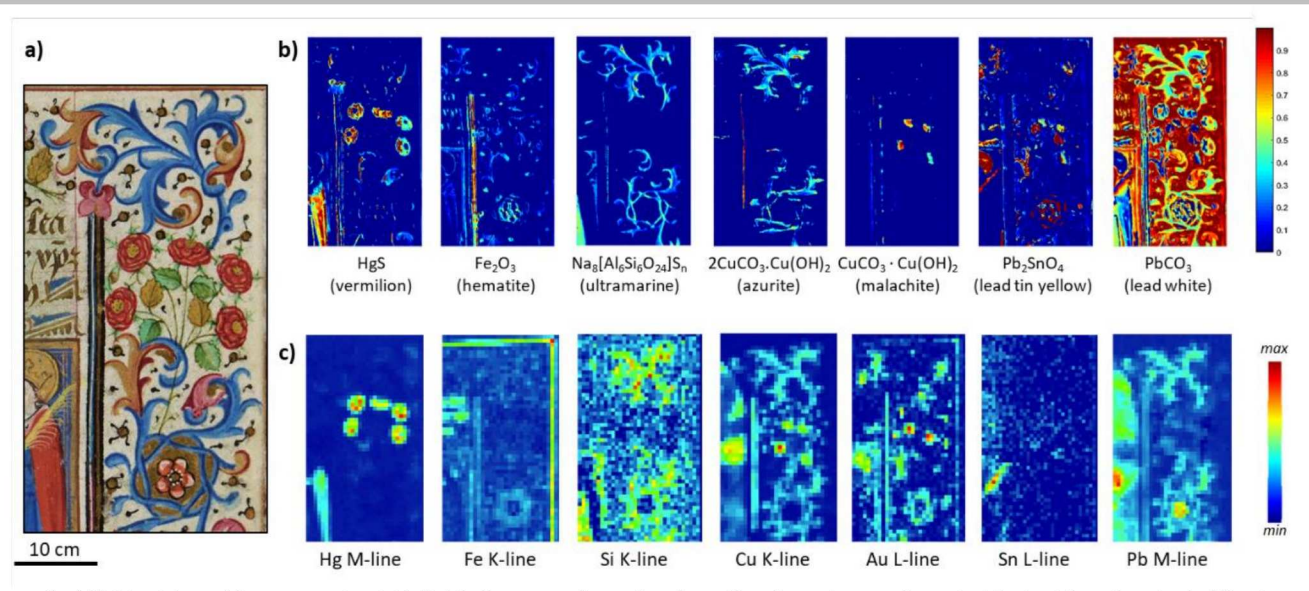


Figure 3: a) Visible picture of the area analyzed; b) Distribution maps of vermilion, hematite, ultramarine, azurite, malachite, lead tin yellow, lead white pigments extracted from hyperspectral datacube using proposed approach; c) Elemental map distribution of mercury, iron, silicon, copper, gold, tin and lead from XRF scanning of the same area.

The spectra of the green foliage and leaves are characterized by a peak reflectance around 535-540 nm and a slow rise from 800 nm (Fig. 4b). These spectral features point toward the use of Cu-containing pigment, a hypothesis confirmed by the presence of Cu identified as the primary element by XRF (Fig. 3c). Malachite (CuCO₃.Cu(OH)₂) was used to obtain the best fit with our experimental data (Fig. 4b) although verdigris or copper resinate could alternatively be present as they have similar spectral responses. This Cu-based pigment was not found alone in the bright green area: lead-tin yellow is also identified in point 2, in Fig. 4c, the two pigments found respectively with a 43%, 47% weight ratios. The 2D pigment maps indicate that there is a clear distribution correlation between the lead-tin yellow and the relatively low but still observable Sn XRF signal identified in the same area. Alternatively, these data could suggest a mixture of a Cu-blue pigment, such as azurite, mixed with the yellow to create the bright green. [36]

As the database used to calculate pigment ratios is determined *a priori*, pigment references can be missing, and thus some pixel spectra can be poorly reconstructed. In order to identify unsuccessful pixel spectrum fitting the root mean square error (RMSE) is calculated on a pixel basis following:

$$RMSE = \sqrt{\frac{\sum_{\lambda=1}^{P} ||R_{Obs,\lambda} - R_{Reconst,\lambda}||_{2}^{2}}{P}}$$

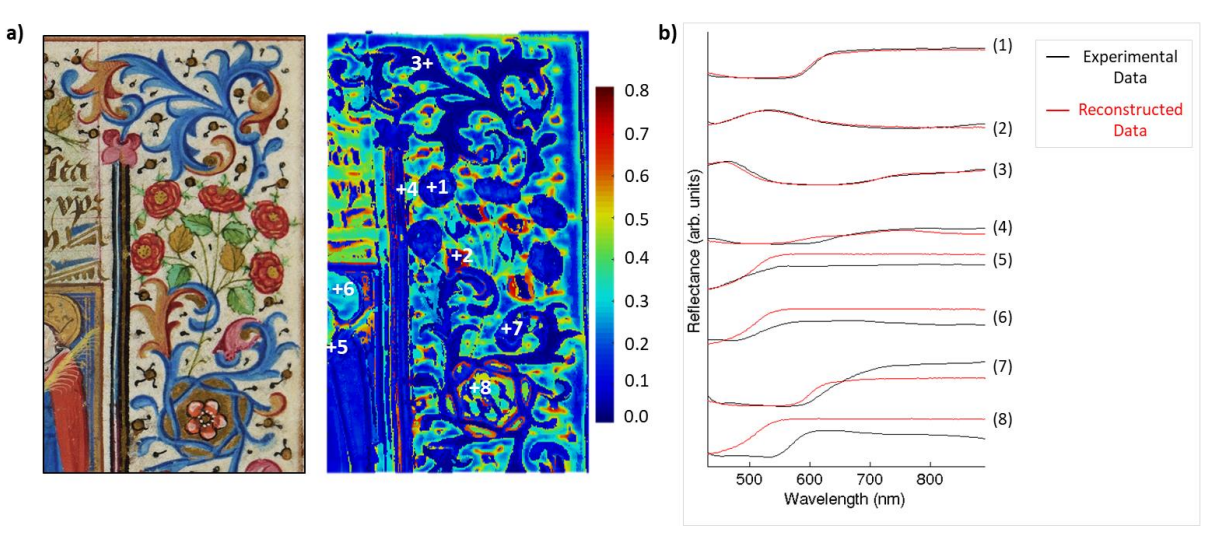
where λ is the wavelength, and $R_{\text{Obs},\lambda}$ and $R_{\text{Reconst},\lambda}$ the observed and reconstructed reflectance spectra, respectively.

The results of the RMSE calculation are presented in Fig. 4a. Low RMSE fitting results are correlated with correct estimation of the expected pigments. Besides the shape edges, and the paper support, high RMSE values may be observed in:

- 1) gilded areas: they were poorly fit to the data (point 6, Fig. 4b) due to specular reflections, a limitation of this approach which models diffuse reflections only.
- 2) the red flower area surrounded by a gilded macaroon at the bottom right of the image (point 8, Fig. 4b). With an inflection point around 565 nm, the pigment present is most likely red lead (Pb_3O_4). [37] This identification may be corroborated by the presence of high content of lead via XRF.
- 3) the pink colored decorations (point 7, Fig. 4b). With an XRF spectrum dominated by Ca signal and a broad asymmetric absorption band centered at 560 nm, these features point toward the use of a pink dye, perhaps brazilwood precipitated on a chalk substrate. [36]

As red lead and brazilwood are missing from our reference library, the poor reconstructions where these pigments are present highlights a second limitation of the nonlinear unmixing approach: for the method to be successful, each pixel of the image must be composed of pigments also present in the database. Conversely, since high RMSE values were encountered only in areas with missing reference spectra, this confirms that the proposed approach does not over-fit the data with the references available.

WILEY-VCH COMMUNICATION



	Vermilion	Ivory Black	Lead Tin	Verdigris	Azurite	Ultramarine	Malachite	Hematite	Lead White	RMSE
point 1	1.00	0.00	0.00	0.00	0.00	0.00	0.00	0.00	0.00	0.0247
point 2	0.00	0.00	0.47	0.00	0.00	0.00	0.42	0.00	0.11	0.0233
point 3	0.00	0.00	0.00	0.00	0.36	0.23	0.00	0.00	0.41	0.0228
point 4	0.00	0.00	0.00	0.00	0.00	0.00	0.00	1.00	0.00	0.0547
point 5	0.00	0.00	0.84	0.00	0.00	0.00	0.00	0.00	0.16	0.182
point 6	0.00	0.00	0.89	0.00	0.00	0.00	0.00	0.00	0.11	0.2333
point 7	1.00	0.00	0.00	0.00	0.00	0.00	0.00	0.00	0.00	0.1743
point 8	0.00	0.00	1.00	0.00	0.00	0.00	0.00	0.00	0.00	0.3203

Figure 4. a) Visible picture and RMSE map of the area analyzed, points of interest are represented by a white cross; b) Comparison of experimental data (black plot) with reconstructed data (red plot) of the pixel of interest detailed in (a); c) Table providing the proportion of reference pigments found in each pixel of interest together with the associated RMSE value.

We have demonstrated a novel quantitative unmixing algorithm using deep neural networks for classification and gradient descent approaches. Quantification opens new possibilities to account for effects not often considered when studying real works of art (yellowing, pigment fading, increased transparency of the paint, particle size). On a HSI dataset acquired from a medieval manuscript, our results are shown to be consistent with complimentary elemental information obtained by XRF. While the approach was successful for the red, blue and green paint layers in the examined manuscript, poor fits were due to lack of some spectral references. To account for this, further work is underway to provide a comprehensive database of absorption and scattering coefficient for pigments and dyes for the use in KM unmixing models. This approach will also be extended to layered structures in paintings by fusing our analyses with analytical systems that probe depth in paintings (e.g. optical coherence tomography).

Acknowledgements

This collaborative initiative is part of NU-ACCESS's broad portfolio of activities, made possible by generous support of the Andrew W. Mellon Foundation. The authors would like to thank Jessica Chloros and Valentine Talland Associate Objects Conservator at the Isabella Gardner Museum (Boston, USA) for motivating non-invasive analyses on the illuminated manuscript.

References

- C. Fischer and I. Kakoulli, Studies in Conservation, vol. 51, no. sup1, [1]
- M. Kubik, Physical Techniques in the Study of Art, Archaeology and Cultural Heritage, D. Creagh, D. Bradley, vol. 2, pp. 199-259, 2007
- H. Liang, Applied Physics A, vol. 106, no. 2, pp. 309-323, Feb 2012.
- M. Alfeld and L. de Viguerie, Spectrochimica Acta Part B: Atomic Spectroscopy, vol. 136, pp. 81–105, 2017. [4]
- J.K. Delaney, K.A. Dooley, R. Radpour, I. Kakoulli, Scientific Reports, vol. 7, no 1, p. 15509, 2017. [5]

- F. Daniel, A. Mounier, J. Perez-Arantegui, C. Pardos, N. Prieto-Taboada, S. Fdez-Ortiz de Vallejuelo, and K. Castro, Microchemical Journal, vol. 126, pp. 113-120, 2016.
- C. Cucci, J.K. Delaney, M. Picollo, Acc. Chem. Res., 49, pp. 2070-[7] 2079, 2016.
- A. Favero, J. Mass, J.K. Delaney, A.R. Woll, A.M. Hull, K.A. Dooley, et al. Herit. Sci., 5, p. 13, 2017.

 A. Mounier and F. Daniel, Studies in Conservation, vol. 60, no. sup1,
- pp. S200-S209, 2015.
- [10] K.A. Dooley, J. Coddington, J. Krueger, D.M. Conover, M. Loew, J.K. Delaney, Anal. Methods, 9, pp. 28-37, 2017.
- A. Cosentino, Heritage Science, 2, p. 8, 2014.
- [12] D. R. Duncan, Proceedings of the Physical Society, vol. 52, no. 3, pp. 390, 1940,
- [13] P. Kubelka and F. Munk, Z. Technol. Physical, vol. 12, pp. 886-892, 1931
- [14] P. Kubelka, J. Opt. Soc. Am., vol. 38, no. 5, pp. 448-457, May 1948. [15] G. Dupuis and M. Menu, Applied physics, vol. 83, no. 4, pp. 469-474,
- [16]
- B. Peric T. Vajzovic H. Liang, K. Keita, The 2nd I'ntl Topical Meeting on Optical Sensing and Artificial Vision, pp. 33-42, 2008.
- [17] G. Latour, M. Elias, and J. M. Frigerio, Appl. Spectrosc., vol. 63, no. 6, pp. 604-610, Jun 2009.
- [18] R. S. Berns and M. Mohammadi, Studies in Conservation, vol. 52, no. 4, pp. 299-314, 2007
- R. S. Berns and M. Mohammadi, Color Research and Application, vol. [19] 32, no. 3, pp. 201-207, 2007
- [20] Y. Zhao, R. Berns, L. A. Taplin, and J. Coddington, in Proc. SPIE 6810, 03 2008.
- [21] R. S. Berns, J. Krueger, and M. Swicklik, Studies in Conservation, vol. 47, no. 1, pp. 46–61, 2002. Y. Zhao, Ph.D. thesis, Thesis. Rochester Institute of Technology, 2008.
- [22]
- W. Zhao and S. Du, IEEE Transactions on Geoscience and Remote Sensing, vol. 54, no. 8, pp. 4544-4554, Aug 2016.
- [24] B. Grabowski, W. Masarczyk, P. Glomb, and A. Mendys, Journal of Cultural Heritage, 2018.
- Y. Chen, X. Zhao, and X. Jia, IEEE Journal of Selected Topics in [25] Applied Earth Observations and Remote Sensing, vol. 8, no. 6, pp.
- 2381–2392, June 2015. Y. Chen, Z. Lin, X. Zhao, G. Wang, and Y. Gu, IEEE Journal of [26] Selected Topics in Applied Earth Observations and Remote Sensing, vol. 7, no. 6, pp. 2094-2107, June 2014
- L. Wei F. Zhang W. Hu, Y. Huang and H. Li, Journal of Sensors, vol. 2015. 2015.

WILEY-VCH COMMUNICATION

- K. Makantasis, K. Karantzalos, A. Doulamis, and N. Doulamis, in 2015 IEEE International Geoscience and Remote Sensing Symposium (IGARSS), July 2015, pp. 4959–4962.
- [29] J. Yue, W. Zhao, S. Mao, and H. Liu, Remote Sensing Letters, vol. 6, no. 6, pp. 468-477, 2015.
- R. Guo, W. Wang, and H. Qi, in 2015 7th Workshop on Hyperspectral Image and Signal Processing: Evolution in Remote Sensing (WHISPERS), June 2015, pp. 1–4.
 E. Pouyet, N. Rohani, A. Katsaggelos, O. Cossairt, and M.Walton, Pure [30]
- [31] and Applied Chemistry, 01 2018.
- M. Aly, Technical Report, Caltech, 01 2005.
- G. Tsoumakas and I. Katakis, International Journal of Data Warehousing and Mining, vol. 3, pp. 1-13, 09 2009.
- J. H. Nobbs, "Kubelka-munk theory and the prediction of reflectance," Review of Progress in Coloration and Related Topics, vol. 15, no. 1, pp.
- C. Kwak and A. Clayton-Matthews, Nursing research, vol. 51, no. 6, pp. [35] 404-410, 2002.
- J.K. Delaney, P. Ricciardi, L.D. Glinsman, M. Facini, M. Thoury, M. [36]
- M. Aceto, A. Agostino, G. Fenoglio, A. Idone, M. Gulmini, M. Picollo, P. Ricciardi, J.K. Delaney, Analytical Methods, 6, 1488-1500, 2014.

 A. Roy, v.2, National Gallery of Art, Washington, DC, 1993.

 Y. LeCun, Y. Bengio, and G. Hinton, vol. 521, pp. 436-44, 05 2015. [37]
- [38]
- [39]
- D. P. Kingma and J. Ba, CoRR, vol. abs/1412.6980, 2014. F. Chollet, "keras," 2015. [40]
- [41]
- M. Abadi et al., 2015, Software available from tensorflow.org.
- J. Snyman, Applied Optimization. Springer, 2005.